ISSN 1063-7710, Acoustical Physics, 2011, Vol. 57, No. 5, pp. 730–736. © Pleiades Publishing, Ltd., 2011.

ACOUSTIC SIGNAL PROCESSING AND COMPUTER SIMULATION

Numerical Simulation of Evaluation of Surface Breaking Cracks by Array-Lasers Generated Narrow-Band SAW[1]

Dong Li-ming, Ni Chen-yin, Shen Zhong-hua, and Ni Xiao-wu

College of science, Nanjing University of Science and Technology, Nanjing, 210094 China

e-mail: shenzh@mail.njust.edu.cn

Received November 18, 2010

Abstract—Most of the factors limiting the extensive application of laser-based ultrasonic for nondestructive evaluation of surface breaking crack are its poor sensitivity, low efficiency relative to conventional contact ultrasonic methods and limit on the dimension of the cracks. For this reason, a new technique that multiple-pulse narrow-band ultrasound generated by laser arrays has been proposed. It is found that crack detection dependent on spectrum of narrow-band ultrasound generated by laser arrays can be operated with low amplitude requirements. In this paper, the narrow-band ultrasound generated by pulse laser arrays interacting with surface breaking cracks has been simulated in detail by the finite element method (FEM) according to the thermoelastic theory. The pulsed array lasers were assumed to be transient heat source, and the surface acoustic wave (SAW) which propagating on the top of the plate was computed based on thermoelastic theory. Then the frequency spectrums of both reflected waves by crack and transmission ones through crack were compared with the direct waves. Results demonstrate that multiple-frequency components of the narrow-band ultrasound were varied with change of the depth of surface breaking cracks significantly, which provides the possibility for precise evaluation of surface breaking cracks.

Keywords: frequency spectrum, narrow-band SAW, array-lasers, surface breaking crack, FEM.

DOI: 10.1134/S1063771011050216

1. INTRODUCTION

Laser based ultrasonic inspection techniques have emerged as a powerful tool in the field of crack evaluation [1–4]. The ability to operate remote from the sample surface, the high fidelity of the detection system, and multiple propagation modes have led to the success of this technology in laboratory tools. The surface acoustic wave (SAW) is suitable for surface crack evaluation, due to its high sensitivity to surface crack, and the Pulsed-echo and pitch-catch techniques in the far field are the main techniques used in surface breaking crack NDE, using laser generated SAWs. Generally, single laser source is applied to generate SAW, whose spectrum and amplitude changes are detected to evaluate the surface crack, especially the amplitude change when the SAW interacts with the surface breaking crack [5–7]. The accuracy of these methods relies on the signal to noise ratio, and the change of SAW amplitude is too small to be identified reliably when the crack size is much smaller than the wavelength of the Rayleigh wave, as a result, this techniques are limited to surface breaking crack measurement.

In an effort to increase the sensitivity of laser based ultrasonic systems, especially for small surface breaking cracks evaluating, the effect of using a spatially modulated array of laser sources has been investigated [8–9]. What is known to all, an increase of signal amplitude in appropriate reduction of the optical detection bandwidth will improve the sensitivity of the whole system. While generation from a single short laser pulse typically leads to broad band acoustic signals, an array of sources can be phased appropriately to obtain strong narrow band signals [10] which improve the Signal-Noise Ratio to increase the sensitivity significantly. What's more, the centre frequencies of the multiple harmonics are determined by the initial-set parameters of the array-lasers, which provide a standard of the measurement for the depth of the crack. Meanwhile, it provides a convenience for the selection of the most commercially available transducers, which exhibit high response to various frequency ranges. Therefore, the waves with different center frequency have different depth of penetration under surface, which can also been applied to detect both surface and sub-cracks.

The idea of generating narrow-band acoustic signals has been implemented in various ways including using the interference pattern from two intersecting laser beams [11–13], repetitive illumination by a lenticular array [14], an optical-fiber-guided laser array [15], a diffraction grating with a lens system [16], and illumination through periodic surface masks [17]. The

[1] The article is published in the original.

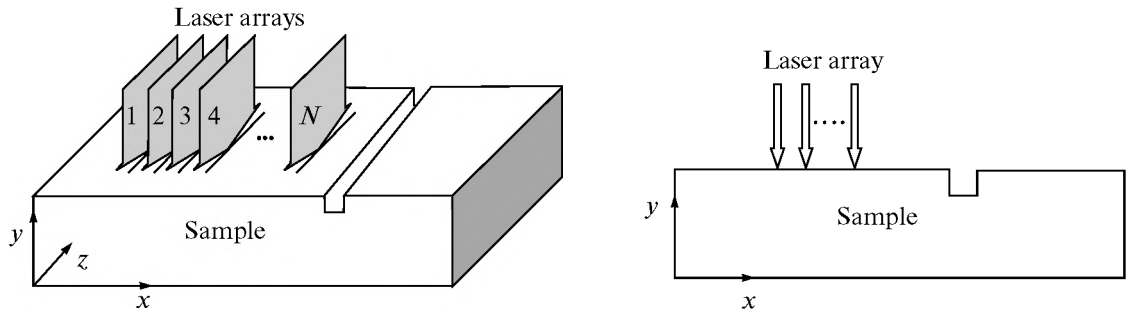

Fig. 1. Schematic diagram of the sample irradiated by the focused laser array line sources: (a) three-dimension; (b) two-dimension.

parameters of laser arrays must be considered to control the band-width and the frequency during the generation of narrow-band ultrasound. However, there are few papers having reported the method of utilizing the frequency spectrum of narrowband SAWs to detect the surface breaking cracks so far. So in this paper, the narrow-band ultrasound generated by pulse laser arrays interacting with surface breaking cracks on aluminum plates has been simulated in detail by the finite element method (FEM) according to the thermoelastic theory. The spectrums of both reflected waves by crack and transmission ones through crack were compared with the direct waves, and the effect of the narrowband SAWs interacting with cracks of different depth is studied.

2. BASIC THEORY AND NUMERICAL MODE

2.1. Thermal Conduction Theory

Both three-dimensional and two-dimensional geometries of laser array irradiation on the top surface of the aluminium plate with the surface breaking crack are schematically shown in Fig. 1. The line sources from array lasers parallel to each other and the surface crack are considered, in addition, the test specimen is a homogeneous, isotropic and linearly elastic half-space; thus each line source of laser array can be considered respectively as a two-dimensional plane strain thermoelastic problem shown in Fig. 1b.

When the sample is illuminated by single laser pulse with energy less than the melting threshold of the material, a certain amount of the light energy is reflected and the remaining energy penetrates into the sample, a non-uniform temperature field will be generated, followed by local thermal expansion, which, in turn, generates the stress field and ultrasonic waves. Considering the laser can be expressed by boundary conditions with energy flow because of the small absorbing depth of the laser on metal surface, the classical governing equations can be expressed as:

$$k\nabla^2 T(x, y, t) - \rho c\dot{T}(x, y, \dot{t}) = 0 \quad (1)$$

$$\rho\ddot{\mathbf{U}}(x, y, t) + \beta\nabla T(x, y, t) = \mu\nabla^2\mathbf{U}(x, y, t) + (\lambda + \mu)\nabla(\nabla \times \mathbf{U}(x, y, t)), \quad (2)$$

where $T(x, y, t)$ is the transient temperature distribution, $\mathbf{U}(x, y, t)$ denotes the displacement vector field, k represents the thermal conductivity, β is the thermoacoustic coupling constant and can be expressed as $\beta = (3\lambda + 2\mu)\alpha_T$, α_T is the coefficient of linear thermal expansion.

The normal boundary conditions are listed as follows:

$$-k\frac{\partial T(x, y, t)}{\partial y}\bigg|_{y=h} = I(x, y, t) \quad (3)$$

$$-k\frac{\partial T(x, y, t)}{\partial y}\bigg|_{y=0} = 0, \quad (4)$$

where $I(x, y, t)$ denotes the energy flow due to single source illumination. An appropriate expression for the surface heat deposition in the solid along an infinitely long line can be found in [16]. In order to simplify the models, the energy flow of laser meaning with $I(x, y, t)$ is loaded on the surface of sample, so the y-dependence of laser is excluded from our consideration. The distribution of energy flow of single laser source along x direction in our models has the relation as:

$$I(x, t) \propto f(x) \cdot q(t) \propto \exp(-x^2/a^2)\frac{t}{t_0^2}\exp(-t/t_0), \quad (5)$$

where a is the half-width of the laser source and t_0 is the pulse width of laser, $q(t)$ is the time dependence of the laser pulse power. Then, the longitudinal displacement can be expressed as the convolution of the function $q(t)$ and a function $h(l, t)$ defined as the diffraction impulse response of the single line source in the thermo-elastic regime, which is discussed in [13] in detail:

$$u(l, t) = q(t) \otimes h(l, t), \quad (6)$$

where l is the distance between the probe point and the near edge of the array lasers.

While the array source which generates surface ultrasonic waves at same time is assumed to be multi-

Thermo-physical parameters of aluminium used in the calculation[a]

Absorptivity	Density, (kgm^{-3})	Specific heat ($Jkg^{-1}K^{-1}$)	Thermal conductivity ($Wm^{-1}K^{-1}$)	Thermal expansion coeffi-cient ($10^{-5}K^{-1}$)	Lamé constant	
					λ (10^{10} Pa)	μ (10^{10} Pa)
5.2×10^{-2} $+3\times10^{-5}$ $(T-300)$	$2769-0.22\times T$	$780.3+0.48T$	$249.5-0.08T$	2.31×10^{-5}	5.81	2.61

Note: [a] All listed parameters are in the temperature range $300\ K \le T \le T_m$, and T_m is the melting point of the material.

sources with equal energy, then Eqs. (5) and (6) can be described as:

$$I_N(x,t) \propto \sum_{k=1}^{N} I(x-kd,t) \propto \sum_{k=1}^{n} f(x-kd)\cdot q(t) \quad (7)$$

$$u(l,t) = q(t) \otimes \sum_{k=1}^{N} h(l,t-k\Delta t), \quad (8)$$

where N is the number of the array sources and d is the distance between the sources centre, Δt is the time delay caused by the space d between the array lasers. According to Eq. (8), the frequency spectrum of the waves can be deducted qualitatively with a discrete because of the time delay and the frequency envelope is almost the same with the situation in which single laser source is applied.

The pulsed heat flux is applied on the laser illuminative regime and other edges are assumed to be adiabatic in the thermal analysis. In addition, the boundary conditions at the top surface ($y = h$) is:

$$\mathbf{n}\cdot[\sigma-(3\lambda+2\mu)\alpha T(x,y,t)\mathbf{I}] = 0, \quad (9)$$

where $\mathbf{n}$ is the unit vector normal to the surface, $\mathbf{I}$ is the unit tensor and σ is the stress tensor. In addition to top surface, the restrictive boundary conditions have been placed at the other sides of the model.

In addition, the initial conditions for the temperature field and displacement field are:

$$T(x,y,0) = 300K \quad (10)$$

$$\mathbf{U}(x,y,0) = \left.\frac{\partial \mathbf{U}(x,y,t)}{\partial t}\right|_{t=0} = 0. \quad (11)$$

2.2. Numerical Method

The classical thermal conduction equation for finite elements with the heat capacity matrix $[C]$, conductivity matrix $[K]$, heat flux vector $\{p_1\}$, and heat source vector $\{p_2\}$ can be expressed as:

$$[K]\{T\}+[C]\{\dot{T}\} = \{p_1\}+\{p_2\}, \quad (12)$$

where $\{T\}$ is the temperature vector, and $\{\dot{T}\}$ is the temperature rise rate vector. For wave propagation, ignoring damping, the governing finite element equation is

$$[M]\{\ddot{\mathbf{U}}\}+[K]\{U\} = \{\mathbf{F_{ext}}\}, \quad (13)$$

where $[M]$ is the mass matrix, $[K]$ is the stiffness matrix, $\{\mathbf{U}\}$ is the displacement vector, $\{\ddot{\mathbf{U}}\}$ is the acceleration vector, and $\{\mathbf{F_{ext}}\}$ is the external force vector. For thermoelasticity, the external force vector for an element is $\int_{S_e}[\mathbf{B}]^T[\mathbf{D}]\{\varepsilon_{th}\}dS$, where $\{\varepsilon_{th}\}$ is the thermal strains vector, $[\mathbf{B}]^T$ is the transpose of the derivative of the shape functions, and $[\mathbf{D}]$ is the material matrix.

The procedure employed to solve the thermoelastic coupling equation is the modeling of the sequential field-coupling, whereby the laser arrays generated temperature field is assumed to produce the stress and displacement fields whose fields on the temperature field is assumed to be negligibly small. The full algorithm has been given in a previous paper [18].

3. NUMERICAL RESULTS AND DISCUSSIONS

3.1. Parameters of Laser Arrays and Sample

On the basis of the above-described models, ultrasound waves generated by array lasers are calculated in an aluminum plate with surface breaking crack. The energy of each laser is 13.5 mJ, the duration time t_0 is taken to be 10 ns and the parameters of array lasers with 5 sources are $a = 100$ μm and $d = 1$ mm, where a is the half-width of the line-shaped pulsed laser spot and d is the space between centres of the laser sources, respectively. The 2D plane element models are constructed to simulate the temperature field accordingly. The maximal element size near the affected zone is 0.5 μm, whereas the element size outside the hear-affected zone is 100 μm.Then the following displacement are simulated by replacing the thermal element with an equivalent plane structural element.

During the structural analysis, the nodal thermal loads are provided by the initial thermal analysis. With scheme, which covers the generation and propagation of surface waves, the locations of laser irradiation regimes on the ultrasonic response of the sensed point on the top surface of sample and the effects of the surface breaking cracks, whose depth are taken to be 1, 0.5 and 0.33 mm, respectively, may be studied quanti-

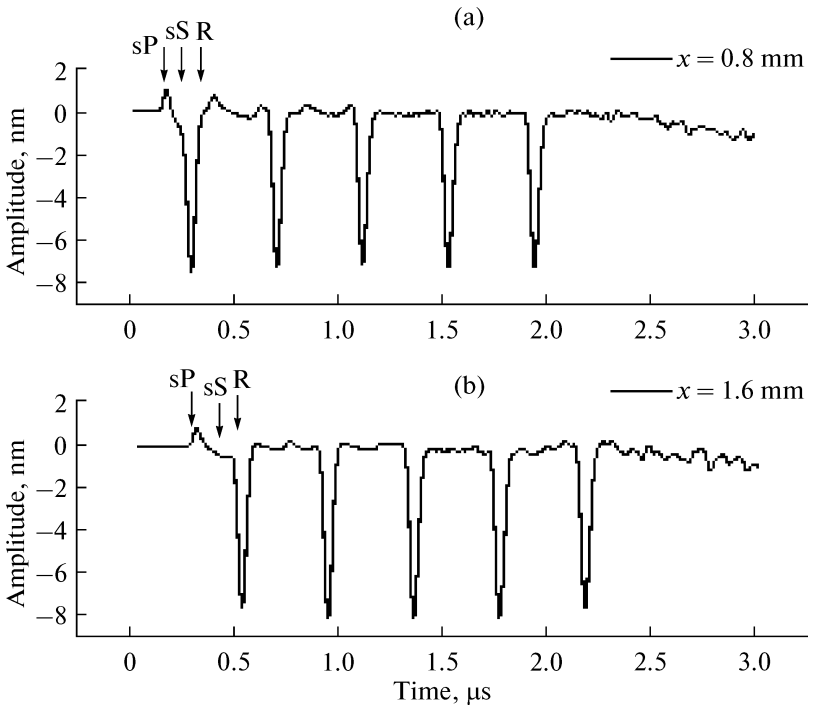

Fig. 2. Vertical displacements on surface generated by 5 lasers array at source-receiver distances of $x = 0.8$ mm and $x = 1.6$ mm, in the 1-cm-thick Al plate.

tatively. The properties of the material used in calculation are listed in table.

3.2. Numerical Results

3.2.1. Waveform of surface waves. In order to understand the effect of generated ultrasound by array-lasers interacting with surface breaking cracks, the vertical surface displacements for the case without a crack in aluminum plate are shown in Fig. 2, which include two SAW signals detected at different distances between right edge of lasers-array and receiver with $x = 0.8$ mm and $x = 1.6$ mm.

The main features of the acoustic signals are three kinds of waves, including skimming longitudinal denoted by sP which is an out-ward displacing monopolar wave, surface shear wave fronts denoted by sS and the main initially negative-going dipolar Rayleigh wave denoted by R. Three kinds of waves are combined together in the near field while the components of sP are separated from sS and R with longer detection distance, which agrees the previous results of single laser source in [19, 20]. Compared with the case of single laser pulse generation, there are five consecutive waves with the same interval in the whole waveform because of the special sources including five array lasers without time delay. What's more, from the waves detected in different points in Fig. 2, the velocity of sP, sS and R calculated on the basis of arrival time are 6040 m/s, 3130 m/s, and 2980 m/s, respectively, in aluminium.

3.2.2. Frequency spectrum analysis of SAWs. Comparing with the continuous broadband ultrasound generated by single laser source, the frequency spectrum of separate waves generated by 5 lasers array is narrowband, which is denoted by solid line. The envelope of the narrowband is almost the same with the frequency spectrum of the surface wave generated by single source, which can be found in Fig. 3 denoted by dotted line. Assuming f is the fundamental frequency and $f = 2.4$ MHz here, it can be found that central frequency of the narrowband waves, which can be called

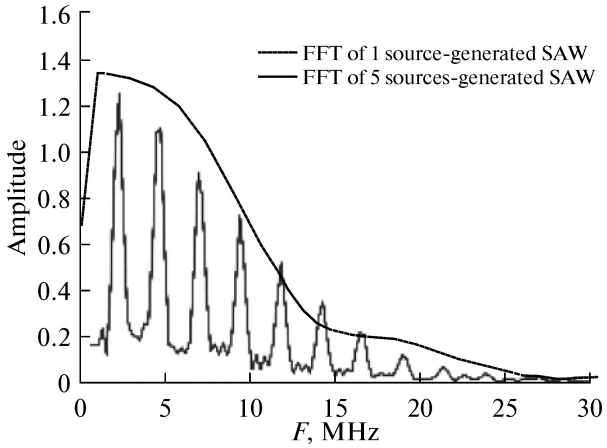

Fig. 3. Frequency spectrum of ultrasound generated by single laser source and 5 lasers array on Al plate.

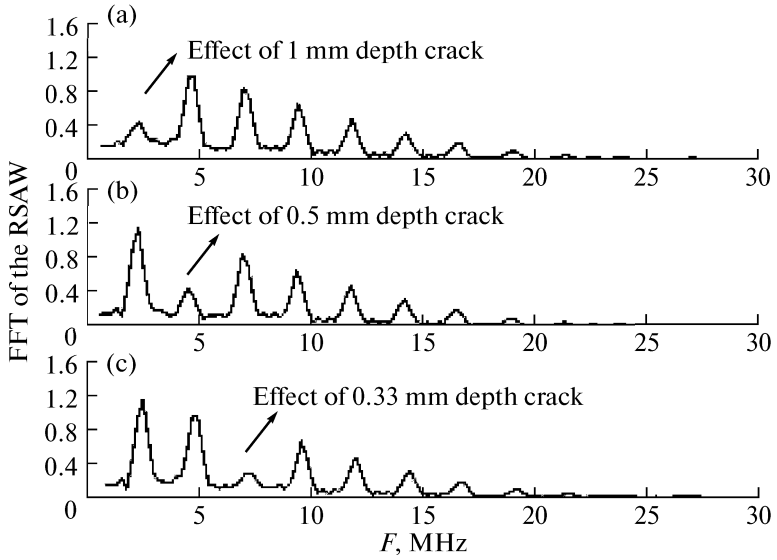

Fig. 4. Frequency spectrums of reflected SAW from crack with depth of (a) 1 mm, (b) 0.5 mm, and (c) 0.33 mm, in 1-cm-thick Al plate.

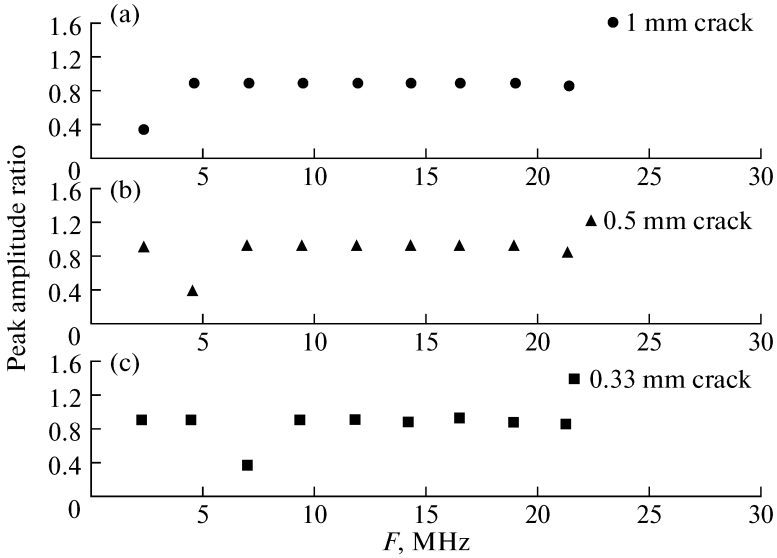

Fig. 5. Diagram of peak amplitude ratio frequency spectrums between reflected waves and direct waves in different crack with depth of 1, 0.5, and 0.33 mm.

second harmonic frequency, third harmonic frequency and so on, is f, $2f$, $3f$, …, nf respectively, whose amplitude gradually reduce to zero coupled with the envelope, so it is known that the narrowband surface acoustic waves can be generated on Al plate by lasers array with wavelength of d, $d/2$, $d/3$, …, d/n.

The narrow-band surface acoustic waves generated by 5 pulse lasers array interacting with surface breaking cracks whose depths are taken to be 1, 0.5 and 0.33 mm, respectively, on aluminum plates have been simulated in detail by the finite element method (FEM) according to the thermoelastic theory. The frequency spectrums of both reflected waves by crack and transmission ones through crack were compared with the direct waves'. Figure 4 denotes the frequency spectrum of the reflected waves from surface crack with different depth of 1, 0.5, and 0.33 mm. The fundamental frequency component in Fig. 4a shows obvious decrease compared with the direct waves. This attenuation effect is mainly because that the wavelength of the fundamental frequency is equivalent to the depth of the surface crack, as a result, the energy of fundamental frequency decrease strongly with it's scattering interacting with the bottom of the crack.

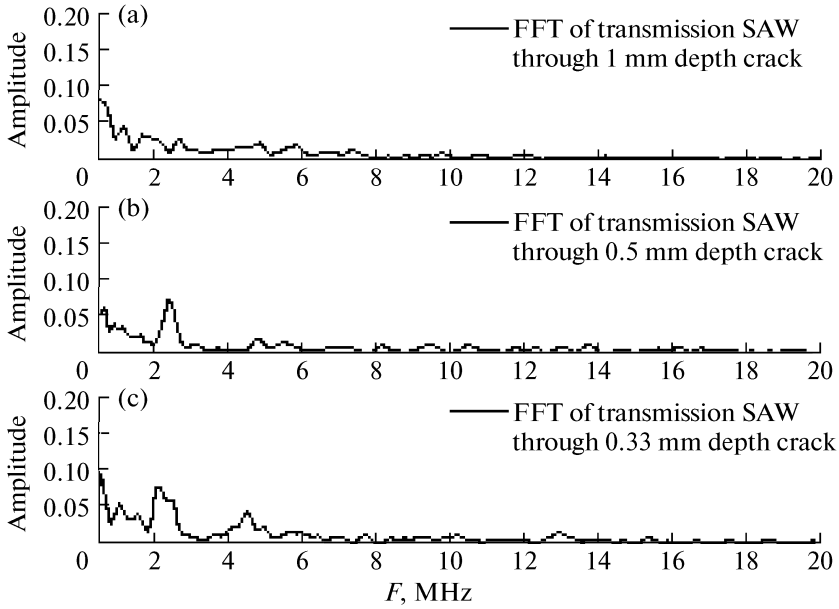

Fig. 6. Frequency spectrums of the transmission waves though the cracks with the depth of (a) 1 mm, (b) 0.5 mm, and (c) 0.33 mm.

Let's consider the situation of smaller cracks with the depth of 0.5 and 0.33 mm whose frequency spectrums are shown in Figs. 4b and 4c. It is found that there are similar attenuation effects of the amplitude corresponding to the reflected waves interacting with alter-depth crack. Specifically, comparing with the situation of direct waves in Figs. 3 and 4, the frequency components of fundamental, second harmonic or third harmonic present attenuated amplitude respectively corresponding to crack depth of 1, 0.5 or 0.33 mm while the amplitude of other frequency components are invariable in reflected waves, which can be also shown clearly from the peak amplitude ratio on centre frequency of reflected waves and direct waves in Fig. 5.

The spectrums of transmission waves through crack with different depth are also observed to compare with the direct waves in Fig. 6. As shown in Fig. 6a, the depth of the crack is 1 mm, which is equivalent to the permeation distance by fundamental frequency ultrasound with the maximal central wavelength in the narrowband signals. As a result, there is no signal detected on the right side of the crack, which indicates that narrowband acoustic waves of all harmonic frequencies are reflected from the left edge of the 1 mm-depth crack. Differently, the ultrasonic signals of fundamental frequency or second harmonic frequency can be detected in the situation when 0.5 and 0.33 mm-depth crack is applied respectively. Therefore, it is confirmed that the narrowband acoustic waves could propagate along the surface over the crack when the wave length at central frequency is larger than the depth of the surface breaking crack.

4. CONCLUSIONS

In this article, the narrowband acoustic waves generated by 5 pulse lasers array interacting with surface breaking cracks with different depth has been simulated in detail by the finite element method according to the thermoelastic theory.

The elastic waves excited by the lasers array in an Al plate are separate narrowband ultrasonic waves, whose envelope is almost the same with the frequency spectrum from single source. And the wavelength of the waves are d, $d/2$, $d/3$, …, d/n corresponding to their central frequency of f, $2f$, $3f$, …, nf, respectively. In addition, the results show that the narrowband surface acoustic waves with different permeation depth on surface are reflected by the surface breaking crack or transmitted though it, which is dependent on the relationship of the depth between the crack and permeation due to the parameters of the lasers array. Therefore, it means that the method for quantitative evaluation of surface cracks is provided making use of the effect of the narrowband acoustic waves generated by lasers array interacting with surface breaking crack.

ACKNOWLEDGMENTS

Authors would like to thank the financial support of this research from the National Science Foundation of China under nos. 60778006 and 60878023, and the Program for New Century Excellent Talents in University (NCET).

REFERENCES

1. E. M. Mfoumou, C. Hedberg, and S. Kao-Walter, Acoust. Phys. **54**, 127 (2008).
2. R. J. Dewhurst, C. Edwards, A. D. W. Mckie, and S. B. Palmer, Appl. Phys. Lett. **51**, 1066 (1987).
3. M. Yu. Izosimova, A.I. Korobov, and O. V. Rudenko, Acoust. Phys. **55**, 153 (2009).
4. A. M. Lomonosov, P. V. Grigoriev, and P. Hess, J. Appl. Phys. **105**, 084906 (2009).
5. S. Dixon, B. Cann, D. L. Carroll, Y. Fan, and R. S. Edwards, Nondestruct. Test. Evaluat. **23**, 25 (2008).
6. J. F. Guan, Z. H. Shen, et al., Acta Photon. **34**, 1128 (2005).
7. M. V. Golub, Acoust. Phys. **56**, 848 (2010).
8. T. W. Murray, M. Marincek, and J. W. Wagner, Ultrasonics Symp., 623 (1993).
9. P. Fomitchov, Liu-Sheng Wang, et al., Proc. SPIE **2921**, 166 (1997).
10. C. Chenu, M. H. Noroy, and D. Royer, Appl. Phys. Lett. **65**, 1091 (1994).
11. A. Harata, N. Nishimura, and T. Sawada, Appl. Phys. Lett. **57**, 132 (1990).
12. K. A. Nelson, R. J. D. Miller, D. R. Lutz, and M. D. Fayer, J. Appl. Phys. **53**, 1144 (1982).
13. M.-H. Noroy, D. Royer, and M. Fink, J. Acoust. Soc. Am. **94**, 1934 (1993).
14. S. W. Allison, G. T. Gillies, D. W. Magnuson, et al., Appl. Opt. **24**, 3140 (1985).
15. Jin Huang, Yasuaki Nagata, Sridhar Krishnaswamy, and J. D. Achenbach, Ultrasonics Symp. 1205 (1994).
16. K. C. Baldwin, T. P. Berndt, and M. J. Ehrlich, Ultrasonics **37**, 329 (1999).
17. I. Arias and J. D. Achenbach, Int. J. Solid Struct. **40**, 6917 (2003).
18. Baiqiang Xu, Zhonghua Shen, Xiaowu Ni, and Jian Lu, J. Appl. Phys. **95**, 2116 (2004).
19. Ji-Jun Wang, Bai-Qiang Xu, Zhong-Hua Shen, Xiao-Wu Ni, and Jian Lu, Jpn. J. Appl. Phys. **47**, 956 (2008).
20. Ji-Jun Wang, Bai-Qiang Xu, and Zhong-Hua Shen, Jpn. J. Appl. Phys. **47**, 956 (2008).